Dzyaloshinskii-Moriya interaction mediated by spin-polarized band with Rashba spin-orbit coupling

A. Kundu and S. Zhang
Department of Physics, University of Arizona, Tucson, Arizona 85721
(Received 9 June 2015; revised manuscript received 6 August 2015; published 21 September 2015)

Dzyaloshinskii-Moriya interaction (DMI) plays a central role in breaking chiral symmetry of magnetic domain wall structure. The recently observed chiral dependence of domain wall structures in ultrathin magnetic films with perpendicular anisotropy indicates the presence of a strong DMI. We calculate the indirect exchange interaction between magnetic ions mediated by spin-polarized conduction electrons with a Rashba spin-orbit coupling. We find the resulting DMI increases with the spin-orbit coupling strength, but decreases with the spin-polarization of the conduction electrons. The estimated DMI magnitude is comparable to the experimental results.

DOI: 10.1103/PhysRevB.92.094434 PACS number(s): 71.70.Gm, 75.30.Et, 75.30.Hx, 75.70.−i

I. INTRODUCTION

Chiral orders of magnetic structure have been observed in bulk materials as well as in ultrathin magnetic films. Various chriral magnetic patterns, such as skyrmion lattice [1–4], helix spins [5,6], handedness of Bloch or Neel walls [7], become interesting topics in topology and magnetism. Interesting dynamics properties of these structures, e.g., dynamics of chiral domain wall [8] and of magnetic skyrmions [9], as well as domain wall motion driven by spin waves [10], have been recently investigated. Microscopic origins of these chiral structures and their dynamic properties have been attributed to Dzyaloshinki-Moriya interaction (DMI) [11,12], whose spin Hamiltonian takes an anisotropic form $H_{\rm DMI} = \sum_{ij} \mathbf{D}_{ij} \cdot (\mathbf{S}_i \times \mathbf{S_j})$, where $\mathbf{S}_i$ is the localized spin at the site i. The DMI requires a broken space inversion symmetry and spin-orbit coupling. Magnetic ultrathin films provide an excellent system for studying magnetic chiral orders since the inversion symmetry is naturally broken as long as substrates and overlayers are made of different materials, and the Rashba spin-orbit coupling [13] at interfaces always exists due to the electrostatic potential differences of contacting materials.

DMI in thin films had been studied previously. Fert and Levy considered the DMI from spin-orbit coupling of impurities [14]. In this model, a conduction electron that is polarized by a magnetic ion $\mathbf{S}_i$ at a position $\mathbf{R}_i$ propagates to an impurity site $\mathbf{R}_0$ whose spin-orbit interaction leads to a spin rotation of the conduction electron such that the conduction electron spin is not parallel (or antiparallel) to $\mathbf{S}_i$. When the conduction electron continues to propagate to another site $\mathbf{R}_j$ and interacts with the magnetic ion $\mathbf{S}_j$, the effective interaction between $\mathbf{S}_i$ and $\mathbf{S}_j$ is no longer symmetric with respect to the interchange of $\mathbf{S}_i$ and $\mathbf{S}_j$. The above magnetic interaction mediated by conduction electrons relies on the existence of heavy element impurities in the film and third-order perturbation on the electron-local spin is needed. Based on tight-binding model, Crépieux and Lacroix had expressed the DMI in terms of spin-orbit parameters at the surface [15]. By symmetry consideration, they were able to construct various forms of DMI with different underlying crystal structure. Another model for the DMI is based on a Rashba band [16]. In this model, the interaction between two magnetic ions are mediated by free electrons, known as the RKKY interaction, except that the free electron band contains the Rashba spin-orbit coupling (RSOC). However, the model is only valid for the interaction between two magnetic impurities in a *nonmagnetic* thin film where the electron bands are not spin-polarized. For ferromagnetic films, such as Ni, the bands are spin polarized and the Rashba interaction is usually much weaker than the exchange interaction. It is thus interesting to extend the conduction-electron mediated DMI to ferromagnetic films where both spin-polarization and RSOC must be included. We noted that the inclusion of both exchange and RSOC has been studied in Ref. [17] in which the effective DM-like coupling is obtained by a different approach (canonical transformation) in some limiting cases.

The present study is also motivated by recent experiments on DMI of ultrathin magnetic films. Gong Chen *et al.* [7] observed the formation of Neel-type of domain wall patterns with a definitive handed helix in perpendicularly magnetized Ni/Co ultrathin films. Since the Bloch wall usually has a lower energy than the Neel wall, the observed Neel wall has been attributed to a large DMI in the film. Another recent experiment [18] directly measured the strength of DMI in Pt/Co and Ni/Co, and found that the DMI are as large as $0.44\,\mathrm{mJ/m^2}$. It would be interesting to see whether the observed strong DMI could be explained by the existence of the well-known interactions: RSOC and the exchange. The paper is organized as follows. In Sec. II, we provide a model Hamiltonian and solve for the conduction electron band structure. In Sec. III, we explicitly evaluate the DMI by using the obtained bands. Analytical results are discussed in limiting cases. In Sec. IV, we calculate DMI for ferromagnetic thin film. In Sec. V, we compare our results with experimental results and discuss the possibility of chiral domain wall, and Sec. VI is dedicated for conclusion.

II. THEORETICAL MODEL

We first consider a two-dimensional ferromagnetic film with a uniformly aligned magnetization $\mathbf{m}$. A model Hamiltonian of the conduction electron,

$$H_0 = -\frac{\hbar^2}{2m}\nabla^{\mathbf{2}} + J\boldsymbol{\sigma}\cdot\mathbf{m} + \alpha(-i\hbar\boldsymbol{\nabla}\times\hat{\mathbf{z}})\cdot\boldsymbol{\sigma}, \qquad (1)$$

describes the exchange coupling between the conduction electron and the magnetization (the second term on the right-hand side of the equation), and RSOC (the last term), where the parameter α characterizes the strength of RSOC,

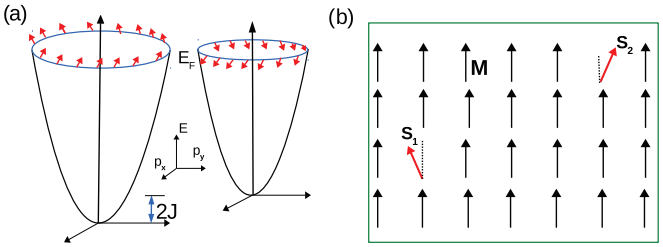

FIG. 1. (Color online) (a) The energy-momentum dispersion relation of Eq. (2) for the magnetization $\mathbf{m}$ parallel to $\hat{\mathbf{z}}$. The arrows represent the directions $\hat{\mathbf{n}}_s$ of electron spin at the Fermi level for the two subbands; see Eq. (3). (b) Two spins $\mathbf{S}_1$ and $\mathbf{S}_2$ make a small deviation from the otherwise uniformly magnetized background.

$\hat{\mathbf{z}}$ is the unit vector along the z axis (perpendicular to the growth direction), and $\boldsymbol{\sigma}$ is the Pauli vector. Equation (1) is the simplest one-body free-electron Hamiltonian that includes two essential properties of ferromagnetic ultrathin films: the spin-polarized bands and spin-orbit coupling.

The solution of Eq. (1) is immediate. The energy-wave vector dispersion relation is

$$\epsilon_{ks} = \frac{\hbar^2 k^2}{2m} + s|J\mathbf{m} + \alpha(\hbar\mathbf{k}\times\hat{\mathbf{z}})|, \tag{2}$$

where $s = \pm 1$ represents two spin-split bands. The momentum-dependent direction of the spin polarization is

$$\hat{\mathbf{n}}_s = s\frac{J\mathbf{m} + \alpha(\hbar\mathbf{k}\times\hat{\mathbf{z}})}{|J\mathbf{m} + \alpha(\hbar\mathbf{k}\times\hat{\mathbf{z}})|}. \tag{3}$$

The wave function is

$$\psi_{ks}(\mathbf{r}) = \frac{1}{\sqrt{A}}e^{i\mathbf{k}\cdot\mathbf{r}}\chi_s(\mathbf{k}), \tag{4}$$

where A is the area of the 2D surface and $\chi_s(\mathbf{k})$ is the spin part of the wave function, which satisfies

$$(\boldsymbol{\sigma}\cdot\hat{\mathbf{n}}_s)\chi_s(\mathbf{k}) = s\chi_s(\mathbf{k}). \tag{5}$$

In Fig. 1(a), we show the dispersion of the two bands and the spin direction at the Fermi surface (circle) for the magnetization perpendicular to the plane of the layer. The spin directions would be more complicated if $\mathbf{m}$ is deviated from $\hat{\mathbf{z}}$.

Having determined the unperturbed bands with the uniform magnetization vector, we now consider two ions whose spin momenta S_1 and S_2 at the positions $\mathbf{R}_1$ and $\mathbf{R}_2$, as shown in Fig. 1(b). The momenta are deviated from the average magnetization $\mathbf{m}$ such that a perturbed Hamiltonian H' is

$$H' = V_0\sum_{i=1,2}\delta(\mathbf{r}-\mathbf{R}_i)\boldsymbol{\sigma}\cdot\Delta\mathbf{S}_i, \tag{6}$$

where $V_0 = Ja_0^2$ is the exchange potential and the δ function represents a zero-ranged exchange interaction between the magnetic moment and the conduction electron, and $\Delta\mathbf{S}_i = \mathbf{S}_i - \mathbf{m}$ is the deviation of the spin $\mathbf{S}_i$ from its average value.

III. DMI MEDIATED BY CONDUCTION ELECTRONS

The first-order correction of H' to the unperturbed Hamiltonian H_0 would give rise to a single-site energy correction to the dispersion relation of Eq. (2). Since we are only interested in the interaction between the two spins of $\mathbf{S}_1$ and $\mathbf{S}_2$, our calculation starts with the second-order perturbation,

$$\delta E = \sum_{\mathbf{k}s,\mathbf{k}'s'}|\langle\psi_{\mathbf{k}s}|H'|\psi_{\mathbf{k}'s'}\rangle|^2\frac{f_{\mathbf{k}s}-f_{\mathbf{k}'s'}}{\epsilon_{\mathbf{k}s}-\epsilon_{\mathbf{k}'s'}}, \tag{7}$$

where $f_{\mathbf{k}s}$ is the Fermi distribution function, which takes the value of 1 (0) if the energy of the state $\mathbf{k}s$ below (above) the Fermi energy, and

$$\begin{aligned}&\frac{A^2}{V_0^2}|\langle\psi_{\mathbf{k}s}|H'|\psi_{\mathbf{k}'s'}\rangle|^2\\ &= \left|\left(\mathbf{p}_1^{ss'}+i\mathbf{p}_2^{ss'}\right)\cdot\left(\Delta\mathbf{S}_1e^{i(\mathbf{k}-\mathbf{k}')\cdot\mathbf{R}_1}+\Delta\mathbf{S}_2e^{i(\mathbf{k}-\mathbf{k}')\cdot\mathbf{R}_2}\right)\right|^2\\ &= \sum_{ij=1,2}\left\{\left(\mathbf{p}_i^{ss'}\cdot\Delta\mathbf{S}_j\right)^2+2\left(\mathbf{p}_i^{ss'}\cdot\Delta\mathbf{S}_1\right)\left(\mathbf{p}_i^{ss'}\cdot\Delta\mathbf{S}_2\right)\right.\\ &\quad\left.\times\cos[(\mathbf{k}-\mathbf{k}')\cdot\mathbf{R}_{12}]\right\}\\ &\quad+2\left(\mathbf{p}_1^{ss'}\times\mathbf{p}_2^{ss'}\right)\cdot(\Delta\mathbf{S}_1\times\Delta\mathbf{S}_2)\sin[(\mathbf{k}-\mathbf{k}')\cdot\mathbf{R}_{12}],\end{aligned} \tag{8}$$

where $\mathbf{R}_{12} = \mathbf{R}_1 - \mathbf{R}_2$, and the real and imaginary parts of the spin matrix element are defined as $\langle\chi_s(\mathbf{k})|\boldsymbol{\sigma}|\chi_{s'}(\mathbf{k}')\rangle \equiv \mathbf{p}_1^{ss'} + i\mathbf{p}_2^{ss'}$. Among all terms in Eq. (8), the asymmetric term in which the exchange between $\mathbf{S}_1$ and $\mathbf{S}_2$ leads to a sign change is the last term containing $\Delta\mathbf{S}_1\times\Delta\mathbf{S}_2$; the rest terms are symmetric with respect to the exchange of $\mathbf{S}_1$ and $\mathbf{S}_2$. Recall that $\Delta\mathbf{S}_i = \mathbf{S}_i - \mathbf{m}$, we may simply write $\Delta\mathbf{S}_1\times\Delta\mathbf{S}_2 = \mathbf{S}_1\times\mathbf{S}_2$ and thus we can readily identify the DMI from Eqs. (7) and (8),

$$E_{\mathrm{DM}} = \mathbf{D}_{12}\cdot(\mathbf{S}_1\times\mathbf{S}_2), \tag{9}$$

where

$$\begin{aligned}\mathbf{D}_{12} = \frac{V_0^2}{8\pi^4}\sum_{ss'}\int d\mathbf{k}\int d\mathbf{k}'\left(\mathbf{p}_1^{ss'}\times\mathbf{p}_2^{ss'}\right)\frac{f_{\mathbf{k}s}-f_{\mathbf{k}'s'}}{\epsilon_{\mathbf{k}s}-\epsilon_{\mathbf{k}'s'}}\\ \times\sin[(\mathbf{k}-\mathbf{k}')\cdot\mathbf{R}_{12}].\end{aligned} \tag{10}$$

In general, the above analytical integration over $\mathbf{k}$ and $\mathbf{k}'$ is very complex.

It is interesting to connect our simple second-order perturbation with more abstract Berry phases in momentum and real space shown in Refs. [19–21]. If we expand our total Hamiltonian in phase space ($\mathbf{R}$, $\mathbf{K}$) as follows:

$$\begin{aligned}H(\mathbf{r}) = H(\mathbf{R},\mathbf{K}) + (\mathbf{k}-\mathbf{K})\cdot\nabla_{\mathbf{K}}H(\mathbf{R},\mathbf{K})\\ +(\mathbf{r}-\mathbf{R})\cdot\nabla_{\mathbf{R}}V(\mathbf{R},\mathbf{K}),\end{aligned} \tag{11}$$

where we have used the fact that spatial dependence of our Hamiltonian only enters in the potential $V(\mathbf{R})$, see Eq. (6), thus $\nabla_{\mathbf{R}}H(\mathbf{R}) = \nabla_{\mathbf{R}}V(\mathbf{R})$. Treating the last two terms as perturbation to the Hamiltonian $H(\mathbf{R},\mathbf{K})$, the second-order perturbation leads to

$$\begin{aligned}\Delta H^{(2)} = \sum_{m\neq n}\frac{\langle m|\frac{\partial V}{\partial R_i}|n\rangle\langle n|\frac{\partial H}{\partial K_j}|m\rangle}{E_m-E_n}+\sum_{m\neq n}\frac{\left|\langle m|(\mathbf{r}-\mathbf{R})\cdot\frac{\partial V}{\partial\mathbf{R}}|n\rangle\right|^2}{E_m-E_n}\\ +\sum_{m\neq n}\frac{\left|\langle m|(\mathbf{k}-\mathbf{K})\cdot\frac{\partial V}{\partial\mathbf{K}}|n\rangle\right|^2}{E_m-E_n},\end{aligned} \tag{12}$$

where m, n represents energy levels corresponding to the unperturbed Hamiltonian $= H(\mathbf{R},\mathbf{K})$. The first term is the

Berry phase term in the mixed representation of the momentum and coordinate space introduced in Ref. [19]. The other two terms describe self-energy corrections.

Before we proceed, we should first comment on several general features of Eq. (10). The direction of $\mathbf{D}$ would consist of the following vector summation:

$$\mathbf{D}_{12} = A\hat{\mathbf{R}}_{12} + B\hat{\mathbf{z}} \times \hat{\mathbf{R}}_{12} + C\hat{\mathbf{m}}. \tag{13}$$

The relative strength of these coefficients, A, B, and C, depend on the RSOC parameter relative to the ferromagnetic exchange J in the energy dispersion, Eq. (2). The last term, $C\hat{\mathbf{m}}$, is unimportant because it does not contribute to the chirality of domain wall structure. The first two terms determine the chiral structure of domain walls; we should discuss later.

Similar to the conventional RKKY interaction, the DMI coefficient $\mathbf{D}_{12}$ displays an oscillatory decay as the distance between two spins $\mathbf{R}_{12}$ increases. Since the denominator in Eq. (10) contains the energy difference between the occupied and unoccupied states, the largest contribution to the integration over $\mathbf{k}$ and $\mathbf{k}'$ comes from the states near the Fermi energy, and thus the sine function in Eq. (9) generates an oscillation with a period of $2k_F R_{12} = 2\pi$. There are two limiting cases where the expression for $\mathbf{D}_{12}$ may be greatly simplified. The first case is that the RSOC is much stronger than the ferromagnetic exchange J. Imamura *et al.* [16] has already explicitly obtained the DMI by using a Green's approach. By setting $J = 0$ in the energy dispersion, Eq. (2), we would arrive at exactly the same expression as derived in Ref. [16]. However, this case is relevant only for a nonmagnetic interface with magnetic impurities, such as Pt or Au thin films doped with dilute magnetic atoms such as Fe and Mn. To address the DMI in ferromagnetic films, e.g., NiCo/Ir or Co/Pt, the ferromagnetic exchange J is usually much larger than the RSOC. Our calculation below will be concentrated in this limiting case.

IV. DMI OF FERROMAGNETIC FILMS

Within the limit of $J \gg \alpha$, we may simplify Eq. (10) by only keeping the lowest order in α. To the zeroth order of α, $\mathbf{D}_{12}$ is identically zero, i.e., there is no asymmetric interaction, and thus we determine the DMI in the first order in α. We further note that Eq. (10) would be identically zero if one takes $\mathbf{p}_1^{ss'} \times \mathbf{p}_2^{ss'}$ to the zeroth order in α and the denominator $\epsilon_{\mathbf{k}s} - \epsilon_{\mathbf{k}'s'}$ to the first order in α. Thus, for the lowest order in α (first order), we should discard the RSOC in the energy dispersion of Eq. (2), i.e.,

$$\epsilon_{\mathbf{k}s} - \epsilon_{\mathbf{k}'s'} = \frac{\hbar^2 k^2 - \hbar^2 k'^2}{2m} + (s - s')J, \tag{14}$$

and calculate $\mathbf{p}_1^{ss'} \times \mathbf{p}_2^{ss'}$ up to the first order in α. After tedious algebra, we find

$$\begin{aligned}\mathbf{p}_1^{ss'} + i\mathbf{p}_2^{ss'} &= -\hat{\mathbf{z}} - is\frac{\alpha\hbar}{2J}(\mathbf{k} - \mathbf{k}') \quad \text{for} \quad \mathbf{s} = \mathbf{s}' \\ &= s\frac{(\mathbf{k} - \mathbf{k}') \times \hat{\mathbf{z}}}{|\mathbf{k} - \mathbf{k}'|} - i\left(\hat{\mathbf{m}} + \frac{\alpha\hbar}{2J}(\mathbf{k} + \mathbf{k}') \times \hat{\mathbf{z}}\right) \\ &\quad \times \frac{(\mathbf{k} - \mathbf{k}') \times \hat{\mathbf{z}}}{|\mathbf{k} - \mathbf{k}'|} \quad \text{for} \quad s \neq s',\end{aligned} \tag{15}$$

and thus we obtain

$$\begin{aligned}\mathbf{p}_1^{ss'} \times \mathbf{p}_2^{ss'} &= -s\frac{\alpha\hbar}{2J}(\mathbf{k} - \mathbf{k}') \times \hat{\mathbf{z}} \quad \text{for} \quad \mathbf{s} = \mathbf{s}' \\ &= -s\left(\hat{\mathbf{m}} + \frac{\alpha\hbar}{2J}(\mathbf{k} + \mathbf{k}') \times \hat{\mathbf{z}}\right) \quad \text{for} \quad s \neq s'.\end{aligned} \tag{16}$$

By placing Eqs. (14)–(16) into Eq. (10), the angular parts of the vectors $\mathbf{k}$ and $\mathbf{k}'$ can be readily integrated out. To make the notations simpler, we make the following variable change, $x = kR_{12}$, $x' = k'R_{12}$, $k_{F\pm} = \sqrt{2m(\epsilon_F \mp J)}/\hbar$, $\Delta = 2mJR_{12}^2/\hbar^2$, $\xi_\pm = k_{F\pm}R_{12}$, $\epsilon_F = \hbar^2 k_F^2/2m$. By using the above definitions and by carrying out the tedious but straightforward algebra, we obtain the main result of the paper,

$$\mathbf{D}_{12} = (\hat{\mathbf{z}} \times \hat{\mathbf{R}}_{12})\left(\frac{2m}{\hbar}\right)^2 \frac{V_0^2 \alpha\hbar}{4\pi^2 R_{12}}[I_0(\xi_+,\xi_-) + I_1(\xi_+,\xi_-)], \tag{17}$$

where I_0 and I_1 represent the intraband and the interband contributions,

$$I_0(\xi_+,\xi_-) = \frac{1}{\Delta}\int_{\xi_-}^{\xi_+} dx \int_0^\infty dx' \frac{G_+(x,x')}{x^2 - x'^2}, \tag{18}$$

and

$$\begin{aligned}I_1(\xi_+,\xi_-) = \frac{1}{\Delta}&\int_{\xi_-}^{\xi_+} dx \int_0^\infty dx' \frac{G_-(x,x')}{x^2 - x'^2 - 2\Delta} \\ &- 4\int_0^{\xi_+} dx \int_{\xi_+}^\infty dx' \frac{G_-(x,x')}{(x^2 - x'^2)^2 - 4\Delta^2},\end{aligned} \tag{19}$$

where

$$G_\pm(x,x') = xx'[xJ_1(x)J_0(x') \pm x'J_0(x)J_1(x')], \tag{20}$$

with $J_0(x)$ and $J_1(x)$ being the Bessel functions of the first kind.

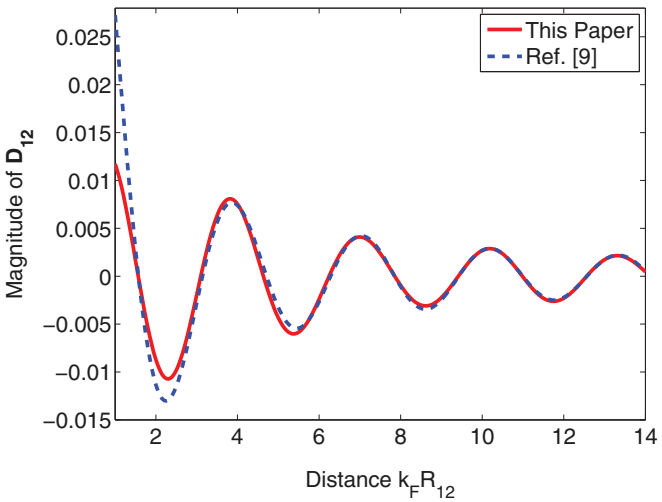

FIG. 2. (Color online) Comparison of the magnitude of $\mathbf{D}_{12}$ [in the unit of $(mV_0^2k_F^2)/(2\pi^2\hbar^2)$] obtained by the limiting expression of Eqs. (21) and (22) with those obtained from Ref. [16]. They are nearly identical.

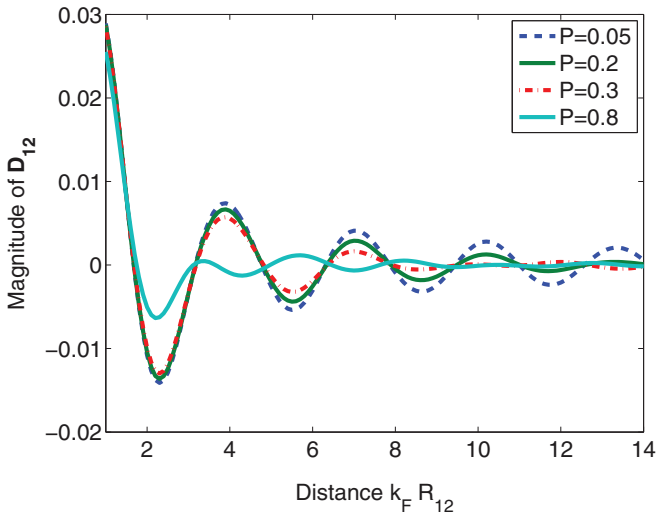

FIG. 3. (Color online) The dependence of the the magnitude of $\mathbf{D_{12}}$ [in the unit of $(mV_0^2k_F^2)/(2\pi^2\hbar^2)$] on the spin polarization P in the weak spin-orbit coupling limit.

One interesting limiting case is the exchange coupling J much smaller than the Fermi energy (but remains much larger than the spin-orbit coupling α). By taking the limit that $\Delta \to 0$ such that $\xi_- = \xi_+ \equiv \xi = k_F R_{12}$, we find that the

$$I_0(\xi) = \int_0^\infty dx \frac{G_+(x,\xi)}{x^2-\xi^2}, \tag{21}$$

$$I_1(\xi) = \int_0^\infty dx \frac{G_-(x,\xi)}{x^2-x'^2} - 4\int_0^\xi dx \int_\xi^\infty dx' \frac{G_-(x,x')}{(x^2-x'^2)^2}. \tag{22}$$

We recall that Imamura *et al.* [16] had also explicitly calculated the DMI in the limit of $J = 0$. In their calculation, the limit is taken at $J = 0$ before a perturbation on the spin-orbit is carried out, i.e., $\epsilon_F \gg \alpha \gg J$. In the present case, we take the limit $\epsilon_F \gg J \gg \alpha$. While the analytical expressions are different, the numerical results for $J = 0$ are nearly identical to those of Ref. [16], as shown in Fig. 2.

When J increases, the spin-polarization $P \equiv J/\epsilon_F$ increases. We numerically integrate Eqs. (18) and (19) as a function of the range $(\xi_+ + \xi_-)/2$ for several different J, as shown in Fig. 3. The oscillation period slightly increases as the polarization increases. The amplitude of the DMI is noticeably smaller for larger P. One may explain such J dependence as follows. For small J, the band has a small spin polarization and thus the interband transition, Eq. (19), contributes most to the DMI. When J becomes large and thus the band is highly spin polarized, the interband transition decreases due to suppression of the density of states of the minority band.

Next, we consider the general case where α and J are arbitrary (but both are smaller than the Fermi energy). In this case, the angular integration in Eq. (10) cannot be performed analytically because the energy dispersion of Eq. (2) contains the relative direction between $\mathbf{k}$ and $\mathbf{m}$. Thus, one must do numerical integration over four variables (magnitudes and angles of $\mathbf{k}$ and $\mathbf{k}'$). To reduce the numerical complexity, we considered the direction of the magnetization being perpendicular to the layer, i.e., $\hat{\mathbf{m}} = \hat{\mathbf{z}}$. In this case the energy denominator is no longer dependent on the direction of the wave vector since $\mathbf{m}\cdot(\mathbf{k}\times\hat{\mathbf{z}}) = 0$. Thus, we can similarly integrate out the angular parts first. The resulting DMI can be expressed below,

$$\mathbf{D_{12}} = -(\hat{\mathbf{z}}\times\hat{\mathbf{R}}_{12})\frac{V_0^2 2m}{4\pi^2\hbar^2 R_{12}^2} I(\xi_+,\xi_-,\alpha), \tag{23}$$

where

$$I(\xi_+,\xi_-,\alpha) = \sum_{s,s'}\int_0^{\xi_s} dx \int_{\xi_{s'}}^\infty dx' \frac{F_{ss'}(x,x')}{E_{ss'}(x,x')}, \tag{24}$$

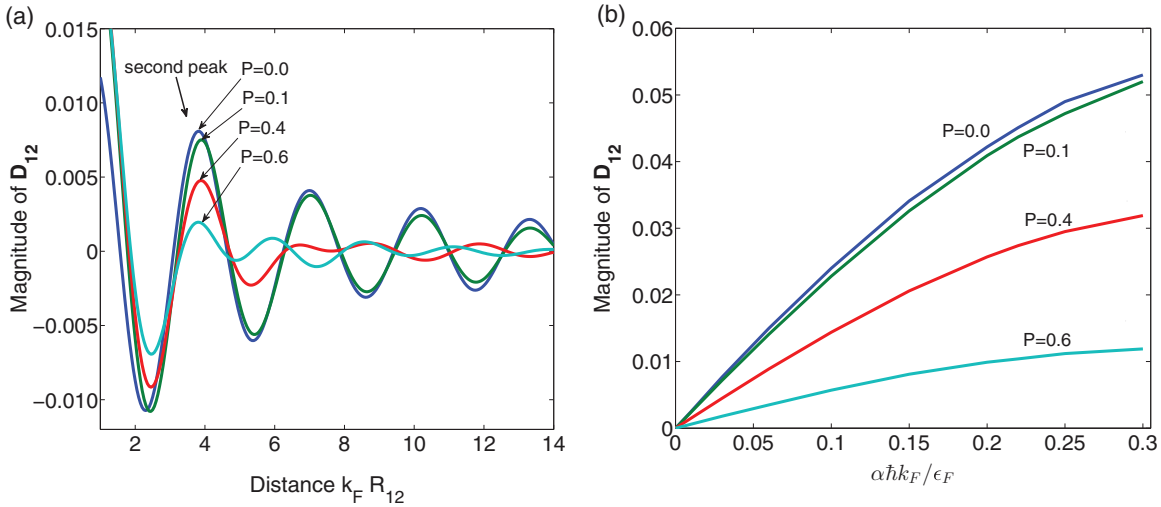

FIG. 4. (Color online) (a) The magnitude of $\mathbf{D_{12}}$ [in the unit of $(mV_0^2k_F^2)/(2\pi^2\hbar^2)$] for several different values of J for a fixed spin-orbit coupling $\alpha\hbar k_F = 0.03$ eV. (b) The magnitude of $\mathbf{D_{12}}$ at the second peak position as a function of α for several different J.

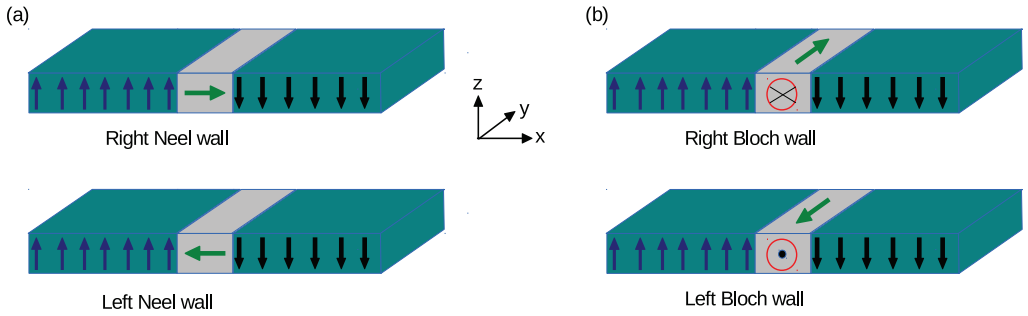

FIG. 5. (Color online) (a) Left (L) and right (R) Neel walls in which the magnetization in the wall $\mathbf{m}_L^N = \cos\theta(x)\mathbf{e}_z - \sin\theta(x)\mathbf{e}_x$ and $\mathbf{m}_R^N = \cos\theta(x)\mathbf{e}_z + \sin\theta(x)\mathbf{e}_x$, where the angle $\theta(x)$ smoothly varies from 0 to π in the wall. (b) Left and right Bloch walls where the magnetization in the wall $\mathbf{m}_L^B = \cos\theta(x)\mathbf{e}_z - \sin\theta(x)\mathbf{e}_y$ and $\mathbf{m}_R^B = \cos\theta(x)\mathbf{e}_z + \sin\theta(x)\mathbf{e}_y$.

where the two functions in the numerator and denominator are as follows:

$$E_{ss'}(x,x') = (x^2 - x'^2) + \frac{2m\alpha\hbar R_{12}}{\hbar^2} \times \left(s\sqrt{\lambda^2 R_{12}^2 + x^2} - s'\sqrt{\lambda^2 R_{12}^2 + x'^2}\right),$$

$$F_{ss'}(x,x') = s\frac{G_+ + G_-}{2\sqrt{\lambda^2 R_{12}^2 + x^2}} + s'\frac{G_+ - G_-}{2\sqrt{\lambda^2 R_{12}^2 + x'^2}},$$

where we have defined $\lambda = J/(\alpha\hbar)$. In Fig. 4 we plot the DMI for various α and J using Eq. (23). In general, the DMI increases significantly with α but decreases with J.

V. DOMAIN WALL STRUCTURE WITH PERPENDICULAR ANISOTROPY

The DMI has a profound effect in domain wall structure of ferromagnetic films, particularly, for ultrathin films with perpendicular magnetic anisotropy (PMA). Since the origin of PMA is the interface spin-orbit coupling, it is natural to assume that these materials, such as Co/Pt and NiCo/x, which possess a large PMA, have a large Rashba spin-orbit coupling, and thus the DMI derived in our previous sections is likely to be applicable to these materials. Indeed, the experimental findings of particular chiral domain wall structure can be at least semiquantitatively explained as we show below.

Domain walls in ultrathin films with PMA have two basic forms known as the Neel and Bloch walls, as depicted in Fig. 5. The arrows between spin-up and spin-down domains represent the average directions of spins of particular types of walls. The energy of the walls consists of exchange, anisotropy, and magnetostatic terms. While the exchange and anisotropy energies (for a fixed-wall width) are the same for these two walls, the magnetostatic energy is higher for the Neel wall due to the presence of the bulk magnetic charge $\rho_m = -\nabla \cdot \mathbf{M} \neq 0$. We can estimate this energy by using the standard ellipsoid model [22] for the Neel wall in which the charge distribution has a geometric shape of an ellipsoid and thus the magnetostatic energy is $(\mu_0 M^2 t\omega)/(\omega + t)$, where, M is the magnetization per unit volume, t is thickness, and ω is the width of domain wall. For the ultrathin film with PMA, $t \ll \omega$, the energy difference between the Neel and Bloch walls is thus simply $E_N - E_B \approx \mu_0 M^2 t$.

Now we include the DMI to the wall energy. Along the direction of the wall shown in Fig. 5, $\mathbf{R}_{12}$ is parallel to $\mathbf{x}$ and hence the DMI vector $\mathbf{D_{12}} = \hat{\mathbf{z}} \times \hat{\mathbf{R}}_{12}$ is parallel to $\hat{\mathbf{y}}$. To estimate the domain wall energy, we only consider the DMI between two nearest spins, denoted as $\mathbf{D_{12}}$. For a Neel wall, the magnetization vector varies continuously along the x axis in the XZ plane $[\mathbf{m}(x) = \cos\theta(x)\hat{\mathbf{e}}_z + \sin\theta(x)\hat{\mathbf{e}}_x]$, and thus the vector product $\mathbf{D_{12}} \cdot [\mathbf{m}(x) \times \mathbf{m}(x + a_0)]$ yields $|\mathbf{D_{12}}|\hat{\mathbf{y}} \cdot [\mathbf{m}(x) \times \partial\mathbf{m}(x)/\partial x]$. Summing over the entire domain wall width, we obtain the Neel wall energy $\pi a_0 |\mathbf{D_{12}}|$ (where a_0 is the lattice constant). For a Bloch wall where the magnetization is $\mathbf{m}(x) = \cos\theta(x)\hat{\mathbf{e}}_z + \sin\theta(x)\hat{\mathbf{e}}_y$, and we immediately see that the dot product $\hat{\mathbf{y}} \cdot [\mathbf{m}(x) \times \partial\mathbf{m}(x)/\partial x] = 0$; i.e, the DMI does not contribute to the Bloch wall energy. For the Neel wall, the DMI lowers the energy for a one-handed helix but raises the energy for other handed helixes, depending on the sign of D_{12} in Eq. (10). If the magnitude of the DMI is large enough, it is possible that the energy reduction in one of helix Neel walls exceeds the energy difference between the Neel wall and Blochl wall estimated above, resulting in a lower total energy of the Neel wall. Indeed, the experiments have shown that the Neel wall with a particular handed helix are formed in NiCo/Pt perpendicular films [7]. Our estimated strength of DMI below would support the formation of the Neel wall.

The order of magnitude of $\mathbf{D}_{12}$ can be readily estimated from Eq. (17). By using plausible values for the Fermi energy $\epsilon_F = 3.0$ eV, the contact potential $V_0 = 0.5$ eV, the lattice constant $R_{12} = 2.5$ Å for Co, and the numerical values of I_0 and I_1 in Fig. 3, we find that the energy reduction is larger than the extra magnetostatic energy of the Neel wall if the spin-orbit parameter α is larger than several percentage of the ϵ_F. From several *ab initio* calculations, the interface RSOC can be of the order of 10–100 meV [23,24]. Two recent experiments on Pt/Co/Ni films [18] and Ni/Pt [7] have estimated the DMI to be 0.4 mJ/m^2 or 0.1 eV per nearest-neighbor pair, which are comparable to the estimation given above.

VI. CONCLUSIONS

We have calculated the DMI interactions of ultrathin magnetic films in the presence of ferromagnetic exchange and the interfacial RSOC. As these two interactions are universal to ferromagnetic films, the present calculation provides an intrinsic mechanism of the DMI. The DMI is directly correlated with the strength of the RSOC and the PMA materials

such as Co/Pt are known to have a large interface spin-orbit coupling. Therefore, our theory provides a natural explanation for the large DMI values of these PMA materials observed experimentally.

ACKNOWLEDGMENT

This work was supported by the NSF (Grants No. ECCS-1127751 and No. 1404542).

[1] N. Nagaosa and Y. Tokura, Nature Nanotech. **8**, 899 (2013).
[2] U. K. Röbler, N. Bogdanov, and C. Pfleiderer, Nature **442**, 797 (2006).
[3] Niklas Rommimg *et al.*, Phys. Rev. Lett. **114**, 177203 (2015).
[4] S. Mühlbauer *et al.*, Science **323**, 915 (2009).
[5] M. Bode *et al.*, Nature **447**, 190 (2007).
[6] S. V. Grigoriev, D. Chernyshov, V. A. Dyadkin, V. Dmitriev, S. V. Maleyev, E. V. Moskvin, D. Menzel, J. Schoenes, and H. Eckerlebe, Phys. Rev. Lett. **102**, 037204 (2009).
[7] Gong Chen *et al.*, Nat. Commn. **4**, 2671 (2013).
[8] S. Emori *et al.*, Nat. Mater. **12**, 611 (2013).
[9] Felix Büttner *et al.*, Nature Phys. **11**, 225 (2015).
[10] Weiwei Wang *et al.*, Phys. Rev. Lett. **114**, 087203 (2015).
[11] I. E. Dzyaloshinskii, J. Phys. Chem. Solids **4**, 241 (1958).
[12] T. Moriya, Phys. Rev. **120**, 91 (1960).
[13] E. I. Rashba, Fiz. Tverd. Tela **2**, 1224 (1960); Sov. Phys. Solid State **2**, 1109 (1960).
[14] A. Fert and P. M. Levy, Phys. Rev. Lett. **44**, 1538 (1980).
[15] A. Crépieux and C. Lacroix, J. Magn. Magn. Mater. **182**, 341 (1998).
[16] H. Imamura *et al.*, Phys. Rev. B **69**, 121303(R) (2004).
[17] K.-W. Kim, H.-W. Lee, K.-J. Lee, and M. D. Stiles, Phys. Rev. lett. **111**, 216601 (2013).
[18] K. Di *et al.*, Phys. Rev. Lett. **114**, 047201 (2015).
[19] F. Freimuth *et al.*, Phys. Rev. B **88**, 214409 (2013).
[20] J. Gayles, F. Freimuth, T. Schena, G. Lani, P. Mavropoulos, R. A. Duine, S. Blugel, J. Sinova, and Y. Mokrousov, Phys. Rev. Lett. **115**, 036602 (2015).
[21] Ganesh Sundaram and Qian Niu, Phys. Rev. B **59**, 14915 (1999).
[22] S. Middelhoek, J. Appl. Phys. **34**, 1054 (1963).
[23] G. Bihlmayer, S. Blügel, and E. V. Chulkov, Phys. Rev. B **75**, 195414 (2007).
[24] M. Nagano *et al.*, J. Phys.: Condens. Matter **21**, 064239 (2009).